Apr 26th - May 3rd

A New Soil Model and Dynamic Soil Properties

Y. Gyoten
Kobe University, Kobe, Japan

K. Mizuhata
Kobe University, Kobe, Japan

T. Fukusumi
Kobe University, Kobe, Japan

H. Hamada
Kobe University, Kobe, Japan

T. Hirose
Kobe University, Kobe, Japan

Proceedings: First International Conference on Recent Advances in Geotechnical Earthquake Engineering and Soil Dynamics, April 26 - May 3, 1981, St. Louis, Missouri

A New Soil Model and Dynamic Soil Properties

Y. Gyoten
Professor of Architectural Engineering, Kobe University, Kobe, Japan

K. Mizuhata
Professor of Architectural and Environmental Planning, Kobe University, Kobe, Japan

T. Fukusumi
Research Associate of Architectural Engineering, Kobe University, Kobe, Japan

H. Hamada and T. Hirose
Graduate Students, Kobe University, Kobe, Japan

SYNOPSIS A series of cyclic triaxial loading tests with varying strain amplitude were performed on samples of clay and sand. Three types of polynomial functions and a hyperbolic function were applied to express the experimental nonlinear hysteresis curve of soils under cyclic loading conditions. These functions were used for the earthquake response analysis of the actual ground containing alluvial clay layer and of the idealized saturated sandy soil ground whose stiffness gradually decreases as the development of pore-water pressure. The results of the dynamic responses and the liquefaction potential were compared for a particular actual site and an idealized site by using the presented models and the hyperbolic function model.

INTRODUCTION

For the aseismic design of building structures, the dynamic characteristics of the subsoil should be clarified. According to the state-of-the-art paper on the stress-strain relationships for soils by Richart,F.E.(1972), for example, the skeleton curve of soils can be adequately represented by a hyperbolic curve formulated by Konder (1963) and Hardin et al.(1972). The presented soil models have been obtained as the product of this skeleton curve and the normalized hysteresis curve expressed by the polynomial functions based on the experimental results and these actual dynamic properties of soils have been used in the earthquake response analysis.

DYNAMIC STRESS-STRAIN RELATIONSHIPS

Skeleton Curve

The skeleton curve used in the analysis is

$$\frac{\tau}{\tau_y}=\left(\frac{\gamma}{\gamma_r}\right)/\left(1+\left|\frac{\gamma}{\gamma_r}\right|\right) \tag{1}$$

in which τ_y is the maximum shear stress:

$$\tau_y=\left[\left(\frac{1+K_0}{2}\sigma'_v\sin\phi'+c'\cos\phi'\right)^2-\left(\frac{1-K_0}{2}\sigma'_v\right)^2\right]^{\frac{1}{2}} \tag{2}$$

In the above equations, γ_r is the reference shear strain, i.e. $\gamma_r=\tau_y/G_0$, σ'_v is the effective vertical stress, K_0 is the coefficient of earth pressure at rest and ϕ' is the effective angle of internal friction. The initial maximum shear modulus G_0 is expressed as the function of σ'_v, K_0 and void ratio e. (Hardin et al.(1972))

Hysteresis Curve

The following polynomial function in the normalized form is considered for loading and unloading curves of the hysteresis loop.

$$\frac{\tau}{\tau_0}=a\left(\frac{\gamma}{\gamma_0}\right)^4+b\left(\frac{\gamma}{\gamma_0}\right)^3+c\left(\frac{\gamma}{\gamma_0}\right)^2+d\left(\frac{\gamma}{\gamma_0}\right)+e \tag{3}$$

The polynomial function was used for the studies on the reinforced concrete structure by Tani,S. et al.(1970) and the structural foundation-ground system by Kitaura, M.(1975). Here the unknown coefficients a,b,c,d,e of the equation are considered as the function of shear strain amplitude γ_0 under cyclic loading. Considering the conditions that both the tangents m of the hysteresis curve and the skeleton curve at strain $\gamma=\gamma_0$ are equal and that $\tau/\tau_0=1$ when $\gamma/\gamma_0=1$ (Fig.1), the following loading and unloading curves of a hysteresis loop are obtained(Model A):

$$\frac{\tau}{\tau_0}=\mp a\left(\frac{\gamma}{\gamma_0}\right)^4+b\left(\frac{\gamma}{\gamma_0}\right)^3\pm\left(\frac{m-1}{2}+2a-b\right)\left(\frac{\gamma}{\gamma_0}\right)^2+(1-b)\left(\frac{\gamma}{\gamma_0}\right)\mp\left(\frac{m-1}{2}+a-b\right) \tag{4}$$

The hysteretic damping of Eq.(4) is

$$h_{eq}=(2/15\pi)[-8a+10b+5(1-m)] \tag{5}$$

Under the same conditions as the above mentioned, by neglecting the second order term or the fourth order term in Eq.(3), the following Eq.(6)(Model B) or Eq.(7)(Model C) are similarly obtained;

$$\frac{\tau}{\tau_0}=\mp a\left(\frac{\gamma}{\gamma_0}\right)^4+\left(2a+\frac{m-1}{2}\right)\left(\frac{\gamma}{\gamma_0}\right)^3-\left(2a+\frac{m-3}{2}\right)\left(\frac{\gamma}{\gamma_0}\right)\pm a \tag{6}$$

the hysteretic damping of Eq.(6); $h_{eq}=8a/5\pi$,

$$\frac{\tau}{\tau_0}=\left(c+\frac{m-1}{2}\right)\left(\frac{\gamma}{\gamma_0}\right)^3\mp c\left(\frac{\gamma}{\gamma_0}\right)^2-\left(c+\frac{m-3}{2}\right)\left(\frac{\gamma}{\gamma_0}\right)\pm c \tag{7}$$

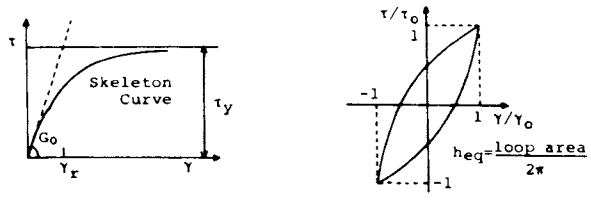

Fig. 1. Skeleton Curve and Normalized Hysteresis Curve

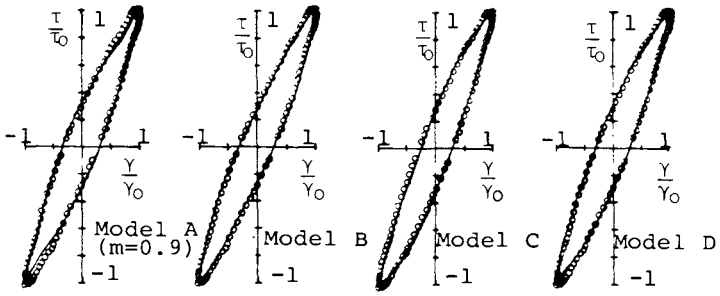

Fig. 2. Comparison of the Calculated and Experimented Hysteresis Curves (Saturated sand, $\sigma_0'=1kg/cm^2$, $\gamma_0=0.112\%$) o: Experiment, ——: Calculated

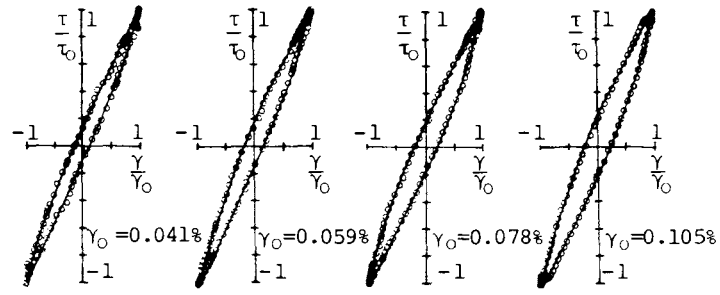

Fig. 3. Variation of Hysteresis Curve with Strain Amplitude (Diluvial clay, Model A(m=0.9), $\sigma_0'=4kg/cm^2$)

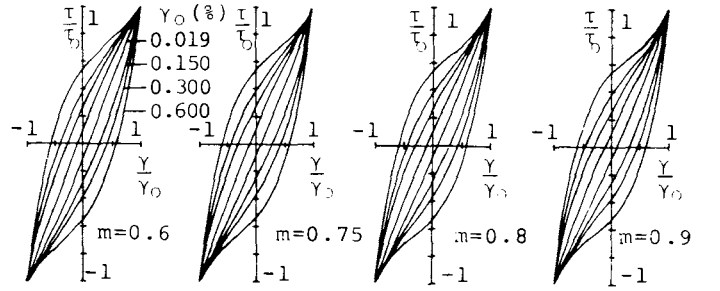

Fig. 4. Variation of Hysteresis Curve with Strain Amplitude (Diluvial clay, Model A, $\sigma_0'=4kg/cm^2$, $H_A=1.57$, $H_B=11.84$, $n=0.534$)

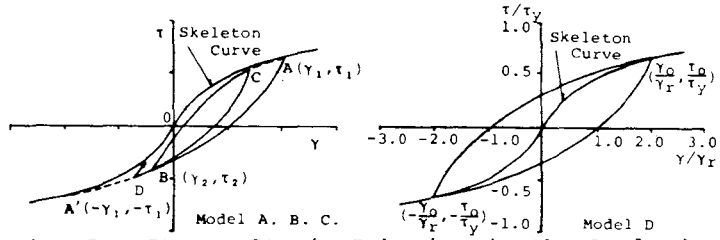

Fig. 5. Stress-Strain Behavior in the Analysis

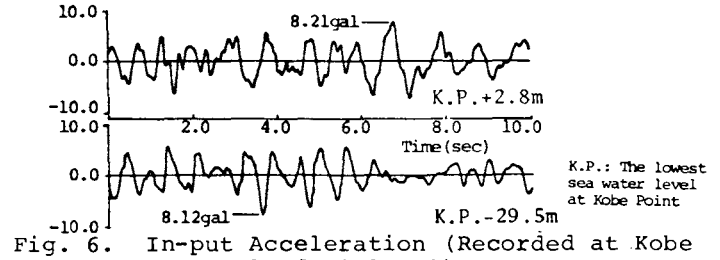

Fig. 6. In-put Acceleration (Recorded at Kobe Port Island 1971, NS)

the hysteretic damping of Eq.(7); $h_{eq}=4c/3\pi$.

Finn et al.(1978) applied the hyperbolic function to the dynamic response analysis. For comparative investigation, the hyperbolic hysteresis curve is also used in this study (Model D):

$$\frac{\tau\pm\tau_0}{2\tau_y}=\frac{\gamma\pm\gamma_0}{2\gamma_r} \Big/ \left(1+\left|\frac{\gamma\pm\gamma_0}{2\gamma_r}\right|\right) \tag{8}$$

$$h_{eq}=\frac{1}{2\pi}\left[8\left(1+\frac{\gamma}{\gamma_r}\right)\left(\frac{\gamma}{\gamma_r}-\log\left|\frac{\gamma}{\gamma_r}+1\right|\right)\Big/\left(\frac{\gamma}{\gamma_r}\right)^2-4\right] \tag{9}$$

In Model A, one condition is lacked to determine the unknown coefficients. Assume that a and b in Eq.(4) can be expressed in the following form referring to the experimental results;

$$a=H_A\gamma_0^n, \quad b=H_B\gamma_0^n+(m-1)/2 \tag{10}$$

and then,

$$h_{eq}=2/15\pi(-8H_A+10H_B)\,\gamma_0^n \tag{11}$$

In the analysis, the hysteretic damping Eq.(11) is taken to approximate the hysteretic damping of Model D, Eq.(9). H_A and m are taken as the following constant value; $H_A=(1+\nu)^n$, $0.5<m<1.0$. For Models B and C, the unknown coefficient is determined corresponding to any arbitrary hysteretic damping, and was determined to be equal to the hysteretic damping of Model D in the analysis. For Model D, h_{eq} can not take any arbitrary value and is expressed by Eq.(11).

Experimental and Calculated Hysteresis Curves

As an example for sand, the calculated hysteresis curves for Models A to D are compared with the experimental hysteresis curve in Fig.2. All the calculated curves for each model seem to well fit the experimental curves. As an example for hard clay, the comparison between experimental curves and calculated curves by Model A(m=0.9) with various shear strain amplitudes is shown in Fig.3. The calculated curves by Model A with various strain amplitudes are shown in Fig.4, where m is taken as 0.6, 0.75, 0.8, 0.9. The value m has little effect on changing the hysteresis curve shape except the vicinity of the extremeties of the hysteresis curve.

Hysteresis Law

The hysteresis law adopted for the polynomial function model is assumed as follows. In Fig.5, up to the first reversal in loading, the stress-strain path follows the skeleton curve, Eq.(1). When the loading is reversed at point A (γ_1,τ_1), the stress-strain curve which connects point A and point A'$(-\gamma_1,-\tau_1)$ with strain amplitude, $\gamma_0=\gamma_1$ is estimated as the subsequent stress-strain curve. On the way toward point A', if the loading is reversed at point B(γ_2,τ_2), a new hysteresis curve which connects point A and point B with strain amplitude, $\gamma_0=|\gamma_1-\gamma_2|/2$. If the loading is not reversed and is continued over point A', the stress-strain path follows the skeleton curve at point A'. According to such a point directive type hysteresis law, the stress-strain curve through points 0→A→B→C→D→···· is drawn under successive loading.

EARTHQUAKE RESPONSE ANALYSIS

Dynamic Response Analysis for an Actual Ground

Models A and D were applied to estimate the dynamic response of a soft ground at Kobe Port Island. The soil properties are shown in Table I, where the initial maximum shear modulus G_0 is evaluated from the measured shesr wave velocity in the down hole method at the site. The lumped mass system with the inherent hysteretic damping at each mass and the additional dissipating damping at the lowest mass (C_C=0.033kg·s/cm, V_S= 200m/s) is solved by the Runge Kutta's Method. The 1st and the 2nd naturalperiods of the ground for the initial shear modulus are; T_1=1.04sec., T_2=0.27sec.. Fig.7 shows the acceleration response spectra of the calculated wave (In-put Max.8.12gal, K.P.-29.5m) and the recorded wave near the surface (Max.8.21gal, K.P.+2.8m) in Fig.6. Both response spectra agree well each other. Fig.8 shows the maximum acceleration and shear strain obtained for the different values of m in Model A. It seems that the hysteresis curve shape is little influenced by the value of m. At the 2nd and 3rd layers of soft alluvial clay, the shear strain response is relatively large (γ_0=0.18%).

Effective Stress Analysis for Sandy Soil Ground

In the earthquake response analysis which takes into account the pore-water pressure development, it is assumed that the stress strain curve degrades step by step due to the increasing of pore-water pressure as shown in Fig.9. The incremental pore-water pressure for one cycle is estimated in the following approximate manner: Corresponding to the resultant shear stress ratio , τ/σ_0', the number of cycles to liquefaction, Nl, is obtained from the S-N curve. And the pore-water pressure ratio, u/σ_0',can be obtained from the pore-water pressure buildup curve expressed by Seed et al.(1976). The S-N curve which was obtained from the laboratory test by K.Tanimoto et al.(1970) in Fig.10 and α=0.7 for the pore-water pressure buildup curve in Fig.11 are used as the analysis data. In the analysis, the continuation of stress and strain before and after the change of effective confining pressure is considered. The initial liquefaction is indicated when the shear stress ratio equals to the dynamic effective angle of shearing resistance. After liquefaction, the effective confining stress is assumed to still reserve 5% of that at the initial state, σ_0'. In addition to the inherent hysteretic damping, 5% of the critical viscous damping proportional to the initial shear modulus is given in the analysis.
Consider the idealized saturated sandy layer of infinite lateral extent resting on horizontal bed rock, which is shaken by horizontal shear waves. The properties of the sandy layers vary with depth (Table II). The stratum of 30m is divided into 10 layers. The water level under the ground of G.L.-1.5m, the coefficient of earth pressure at rest of K_0=0.5 and the in-put acceleration wave of Kobe P.I.(max.100gal, K.P. -29.5m) in Fig.6 are used.
The earthquake responses were obtained by using Models A(m=0.9) to D considering the internal redistribution of pore-water pressure, i.e. the permeability of k=0.1 cm/s which is representative of medium sand, the less permeability of k= 0.01 cm/s and no internal redistribution.

TABLE I. Physical and Mechanical Properties of Ground in Kobe Port Island

	Depth (-m)	Soils	ρ (g/cm³)	e	φ' (degree)	G_0 (kg/cm²)	τ_y (kg/cm²)
7	5.25	sand	1.60	0.456	32.0	640.0	0.095
6	10.50	sand	1.60	0.699	29.0	640.0	0.204
5	15.25	sand	1.80	0.734	31.0	720.0	0.330
4	20.00	sand	1.80	0.807	32.0	720.0	0.463
3	25.50	clay	1.55	1.685	0.0	225.0	0.340
2	31.00	clay	1.55	1.724	0.0	225.0	0.445
1	37.50	sand	1.70	0.980	32.0	650.0	0.780

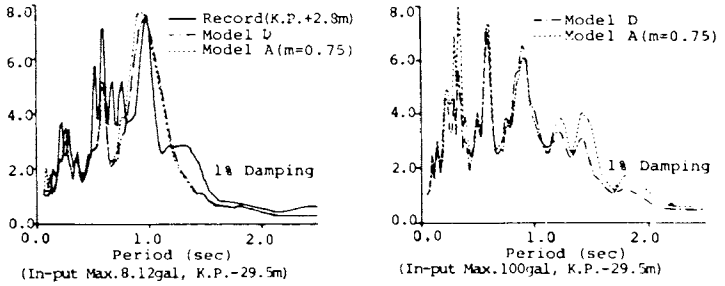

Fig. 7. Acceleration Response Spectra of Analytical Results and Record

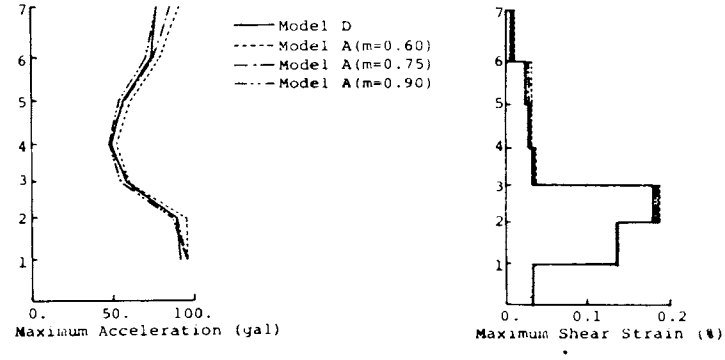

Fig. 8. Maximum Acceleration and Shear Strain Responses (In-put Max.100gal K.P.-29.5m)

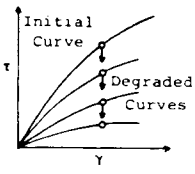

Fig. 9. Degrading of Skeleton Curve

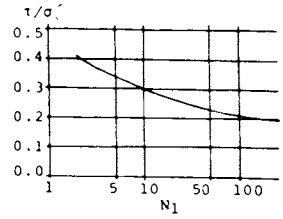

Fig. 10. S-N Curve for Liquefaction in the Analysis (by K.Tanimoto)

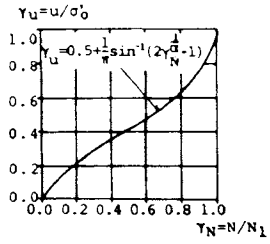

Fig. 11. Ratio of Pore-Water Pressure Buildup (by H.B.Seed)

TABLE II. Physical and Mechanical Properties of Analyzed Ground

	Depth (-m)	G_0 (kg/cm²)	τ_y (kg/cm²)	Parameter
10	3.0	497.4	0.114	ρ:1.9 (g/cm³)
9	6.0	703.5	0.228	
8	9.0	861.6	0.342	e:0.57
7	12.0	995.1	0.456	
6	15.0	1112.4	0.570	φ':39.0 (degree)
5	18.0	1218.6	0.685	
4	21.0	1316.4	0.799	
3	24.0	1407.3	0.913	m_v=5×10⁻³ (cm²/kg)
2	27.0	1492.5	1.027	
1	30.0	1573.2	1.141	

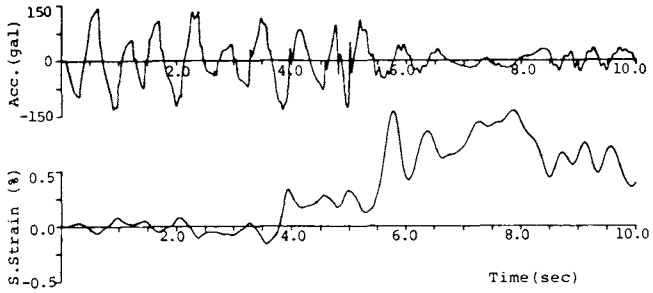

Fig. 12. Acceleration and Shear Strain response at 8th Layer (Model B, k=0.01cm/s)

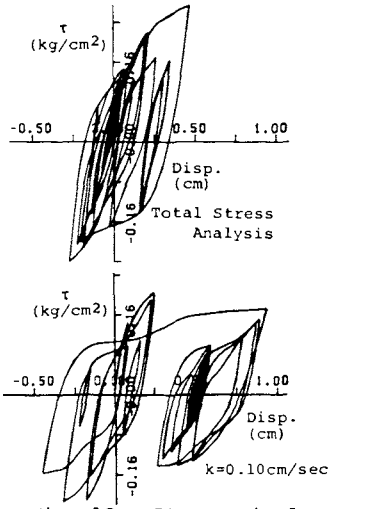

Fig. 13. Stress-Displacement Response Curves (Model B)

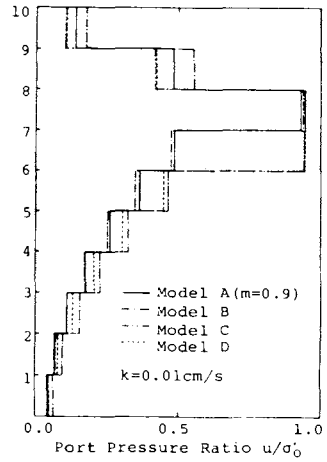

Fig. 14. Maximum Pore-Water Pressure Responses (in 10sec.)

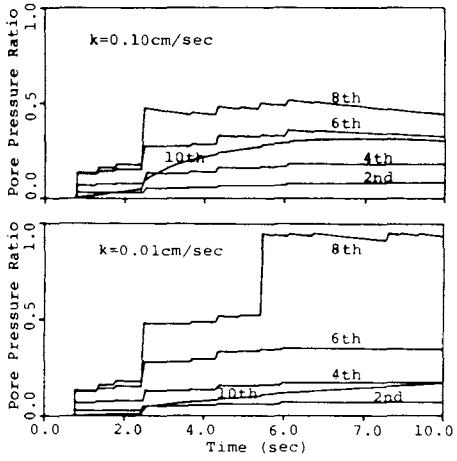

Fig. 15. Computed Development of Pore-Water Pressures during Earthquake (Model B)

Fig.12 shows the responses of acceleration and shear strain at the 8th layer in Model B(k=0.01 cm/s). It can be clearly observed that the acceleration decreases and the shear strain becomes remarkably large after liquefaction at t=5.4sec.. Fig.13 shows the results of the shear stress-displacement curve, which are the examples of both cases of neglecting and considering the pore-water pressure development (k=0.1 cm/s). In the latter case, the liquefaction dose not occur but the displacement tends to drift on one side during earthquake loading. Fig.14 shows the maximum pore-water pressure response along depth in Models A to D (k=0.01cm/s). The results in Models C and D resemble each other and show that both the 7th and 8th layers are led to liquefaction, while it is limited to only the 8th layer in Models A and B. Fig.15 shows the time history of pore-water pressure development for the different permeabilities (k=0.1cm/s and k=0.01cm/s). The redistribution from deeper layers increases the pore-water pressure at surface. While at the 8th layer, the reduction of the pore-water pressure due to the diffusion towards the surface is observed. This tendency is more remarkable for the case of the larger permeability (k=0.1cm/s).

CONCLUSION

The hysteresis curve shapes of soils which vary with strain amplitude are expressed by the presented three types of normalized polynomial functions whose coefficients vary with strain amplitude.

In the analysis, the treatment for Model A including one undeterminated coefficient is different from that for Models B and C, and one of the unknown coefficients H_A was taken as constant, and m is taken as $0.5<m<1.0$. It was found that the results of the earthquake response analysis for the actual ground were almost the same by using Models A and D, and that m has little effect in Model A.

The effective stress analysis for the idealized saturated sandy soil groud was carried out by considering the pore-water pressure development in an approximate way. By comparing the results, for Models A to D, it was found that the maximum responses of stress and acceleration were almost the same, but the maximum responses of shear strain and pore-water pressure were considerably different. In order to simulate the soil behavior after liquefaction, it will be necessary to use more acculate method in estimating the pore-water pressure development.

From the results of effective stress analysis considering the internal redistribution, it can be seen that the redistribution from deeper layer increases the pore-water pressure at surface. This tendency is more remarkable for the case of the larger permeability.

REFERENCES

Finn,W.D.L., G.R.Martion and M.K.W.Lee (1978), "Comparison of the Dynamic Analysis for Saturated Sand", Proc. ASCE Geotech. Eng. Special Conf. on Earth. Eng and Soil Dynamics, ASCE, Vol.1, pp472-491, Pasadena California, June.

Hardin,B.O. and V.P. Drnevich (1972), "Shear Modulus and Damping in Soils: Design Equations and Curves", J.SMFD, Proc. ASCE, Vol.98, No. SM7, July, pp. 667-692.

Seed,H.B., P.P. Martin and J.Lysmer (1976),"Pore-Water Pressure Changes During Soil Liquefaction", J.JGE, Proc. ASCE, Vol. ,No.GT4,323-346

Yoshimi,Y., F.E.Richart,S.Prakash,D.D.Barkan and V.A.Llichev (1977), "Soil Dynamics and its Application to Foundation Engineering", Proc.9th ICSMFE, State-of the Art Report, pp. 605-650.